AIP | Review of Scientific Instruments

Momentum rate probe for use with twophase flows

S. G. Bush, J. B. Bennett, P. E. Sojka, M. V. Panchagnula, and M. W. Plesniak

Citation: Review of Scientific Instruments **67**, 1878 (1996); doi: 10.1063/1.1146992
View online: http://dx.doi.org/10.1063/1.1146992
View Table of Contents: http://scitation.aip.org/content/aip/journal/rsi/67/5?ver=pdfcov
Published by the AIP Publishing

Momentum rate probe for use with two-phase flows

S. G. Bush,[a] J. B. Bennett,[b] P. E. Sojka,[c] M. V. Panchagnula,[a] and M. W. Plesniak[d]
Thermal Sciences and Propulsion Center, School of Mechanical Engineering, Purdue University, West Lafayette, Indiana 47907-1003

(Received 18 September 1995; accepted for publication 1 February 1996)

An instrument for measuring the momentum rate of two-phase flows is described, and design and construction details are provided. The device utilizes a conelike body to turn the flow from the axial to the radial direction. The force resulting from the change in momentum rate of the turning flow is measured using a strain-gage-instrumented cantilevered beam. The instrument is applicable to a wide range of flows including nuclear reactor coolant streams, refrigerants in heating-ventilating air-conditioning equipment, impingement cooling of small scale electronic hardware (computer chips are one example), supercritical fuel injection (in Diesel engines, for instance), and consumer product sprays (such as hair-care product sprays produced using effervescent atomizers). The latter application is discussed here. Features of the instrument include sensitivity to a wide range of forces and the ability to damp oscillations of the deflection cone. Instrument sensitivity allows measurement of momentum rates considerably lower (below 0.01 N) than those that could be obtained using previous devices. This feature is a direct result of our use of precision strain gages, capable of sensing strains below 20 μm/m, and the damping of oscillations which can overwhelm the force measurements. Oscillation damping results from a viscous fluid damper whose resistance is easily varied by changing fluids. Data used to calibrate the instrument are presented to demonstrate the effectiveness of the technique. As an example of the instrument's utility, momentum rate data obtained using it will be valuable in efforts to explain entrainment of surrounding air into effervescent atomizer-produced sprays and also to model the effervescent atomization process. © *1996 American Institute of Physics.* [S0034-6748(96)02405-4]

I. INTRODUCTION

Two-phase flows are present in many areas of science and engineering. The mass flow rates of these flows span a wide range of values, from those in nuclear power plant cooling systems, through supercritical diesel fuel injection, heating-ventilating and air-conditioning (HVAC) refrigerants, and down to impingement jet cooling of electronic components and consumer product aerosols.

The range of momentum rates produced by these applications is also substantial. Previous efforts to measure momentum rate resulted in instrumentation able to serve the needs of those studying high mass flow rate applications; researchers interested in investigating low mass flow rate problems were, unfortunately, without recourse.

In order to overcome this limitation, one approach would be to design a new instrument targeted specifically toward low mass flow rate problems. A better approach is to design an instrument that could, with fairly minor changes, be used to study a wide variety of situations. That more versatile instrument is the subject of this article.

We start with a description of a low mass flow rate application of particular interest to us, then briefly review previous instruments of similar design that were developed for large mass flow rate studies. We next provide design and construction details for our instrument, noting its advantages over previous devices. This is followed by results obtained during a recent study of effervescent atomizer sprays formed from consumer products. Instrument calibration data are then presented that demonstrate the effectiveness of the technique. We end with an analysis of the measurement uncertainties characteristic of the instrument.

Our primary application of this instrument is to liquid atomization (also known as spray formation). Lately we have focused our efforts on effervescent atomization.

Effervescent atomization is an emerging spray technology that has the potential to make spraying many high viscosity fluids effective and economical. For example, new regulatory requirements are aimed at reducing solvent emissions in consumer product spray systems and effervescent atomization is one way of meeting these requirements while retaining advantages such as reliability and energy efficiency.

Sprays produced by effervescent atomizers differ from those produced by conventional injectors (such as plain orifice, pressure swirl, airblast, air-assist, and rotary) because effervescent atomization requires a well-mixed two-phase flow at the atomizer exit orifice. For a detailed discussion of effervescent atomization see Lund *et al.*[1]

Effervescent atomizers often produce sprays with smaller cone angles than those provided by conventional atomizers, thereby suggesting that a smaller quantity of the surrounding gas is entrained. Entrainment is critical in many consumer product sprays, since the carrier solvent must evaporate so that the active ingredient can effectively perform its intended task when it strikes the target.

Recent modeling of the entrainment behavior of effervescent sprays has focused on jet momentum rate. Since ef-

[a]Graduate Research Assistant.
[b]Undergraduate Research Assistant.
[c]Associate Professor.
[d]Assistant Professor.

 0034-6748/96/67(5)/1878/8/$10.00

fervescent sprays are characterized by a two-phase flow at the nozzle exit, calculation of the jet momentum rate is considerably more complicated than in the case of a single-phase (gas) jet. This complication arises from the fact that the velocities of both the atomizing gas and the liquid to be sprayed are required to calculate the spray momentum rate, and these velocities are not available without a constitutive equation or experimental measurements. An instrument capable of directly measuring the momentum rate of a developing spray would serve two purposes. First, the value of momentum rate could be used directly in experimental investigations of entrainment so that phase velocity correlations or individual velocity measurements need not be employed. Second, the momentum rate data could be used to develop phase velocity models that would be incorporated into drop sizing models[1] and into entrainment prediction models.[2]

II. EXPERIMENTAL FACILITY

A. Principle of operation

The momentum rate of an axial two-phase flow, such as a spray, may be measured by converting the axial flow to radial flow. This can be accomplished through the use of a flat plate, an impulse cage, or a conelike device. For example, Giffen and Crang[3] utilized an impulse cage, a plate fitted with vanes that direct the flow radially outward, and a spring balance to measure momentum rate for steam flows exiting 35-mm-diam nozzles. Klingebeil and Moulton[4] also used an impulse cage to measure momentum rate in steam–water mixtures exiting 13-mm-diam tubes. They substituted a load cell for the spring balance of Giffen and Crang. More recently, Deichsel and Winter[5] measured momentum rates of two-phase air–water flows in 1- to 5-mm-diam tubes. Their instrument consisted of a deflection cone and a calibrated load cell to measure the forces generated by the deflected flows.

While the instruments described in Refs. 3–5 are capable of measuring momentum rates for large mass flow rate applications, the measuring apparatus in a low mass flow rate application must, in many cases, resolve forces much smaller than those reported by the authors cited above. For example, the momentum rate resulting from low mass flow rate effervescent sprays is typically in the range of 0.01 to 0.1 N and no commercially available load cell or spring scale can resolve forces of this small magnitude. We therefore incorporated a cantilevered beam instrumented with precision strain gages to measure the appropriate range of forces. As noted below, a wide range of two-phase flows may be studied by installing different beams that have various stiffnesses. Beam stiffness can be easily modified by changing thickness or material. Strain gages having the appropriate range and sensitivity can be obtained from a number of commercial vendors.

The strain-gage-instrumented cantilevered beam was attached to a deflection cone, which turned the two-phase flow from the axial to the radial direction. A flat plate was not employed because of the difficulty in ensuring that the entire flow is deflected radially. An impulse cage was not used, due to the possible influence on the momentum rate measurement of feedstock buildup on the guide vanes. The deflection cone has the additional advantage that the contoured cone routes the flow radially outward, thereby avoiding the problem of flow rebound associated with a flat plate.

The contour of the deflection cone was obtained from the equation of the streamlines for an incompressible stagnation point flow. The deflection cone used in the instrument described here is shown in Fig. 1.

An overall view of the instrument is shown in Fig. 2. Note that the spray is directed horizontally at the deflection cone, resulting in movement of the beam. Beam movement leads to a strain at the root of the beam, which is measured using strain gages.

B. Deflection cone

The contour of the deflection cone shown in Fig. 1 was calculated using White's[6] analysis of axisymmetric, incompressible stagnation point flow. See Appendix B for details. This analysis is based on the similarity solutions of Hiemenz[7] and Homann[8] (as presented by White). The result is a numerical representation of a streamline which can be used in a computer numerically controlled (CNC) machine tool to fabricate the cone. The shape of the cone ensures that the droplet-laden gas impinging on the deflection cone is turned through 90°.

C. Strain gage beam

Our use of a strain gage beam provides two of the key advantages of this instrument. First, modern precision strain gages allow strains as low as 20 μm/m to be accurately measured, thereby facilitating sampling of momentum rates in the mN range. Second, simply substituting one beam-gage assembly for another allows the instrument to operate over a wide range of momentum rates.

The cantilevered beam shown in Fig. 2 is actually an assembly consisting of three parts. The upper and lower rigid portions are designed to create a measurable bending moment at the end of the central strain-sensing beam. The rigid beams are 3.2-mm-thick plate aluminum while the strain-sensing beam is 0.79-mm-thick cold drawn steel. Figure 3

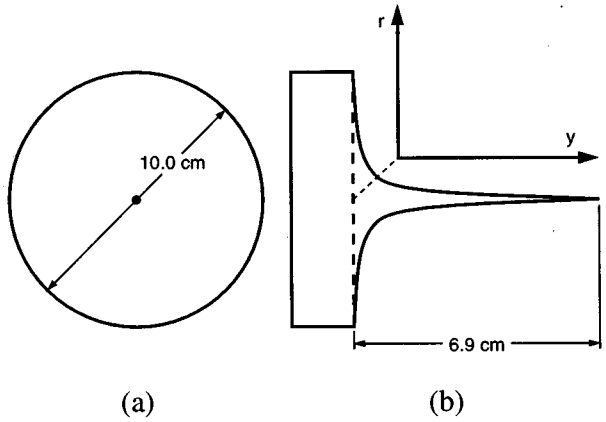

FIG. 1. Deflection cone for use with momentum rate probe: (a) front view; (b) side view.

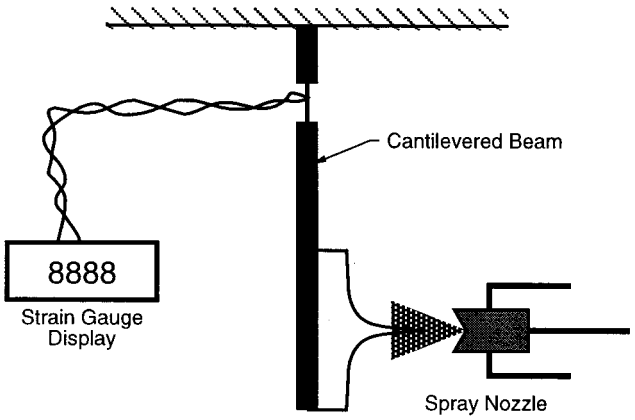

FIG. 2. Schematic of momentum rate probe.

shows the dimensions of these beams. The compound beam configuration was chosen after it was found that a single 3.2-mm-thick aluminum beam was too rigid to allow the use of strain gages for low mass flow rate sprays.[9] Beam deflection calculations showed that the 0.79-mm-thick steel section would result in the appropriate deflection for the given bending moment, while minimizing modifications to the basic instrument design.

The compound beam design concentrates the bending moment in the strain-sensing beam. This can be shown by comparing the beam stiffness, EI, of the two components:

$$EI_{\text{steel}}/EI_{\text{aluminum}}=75. \tag{1}$$

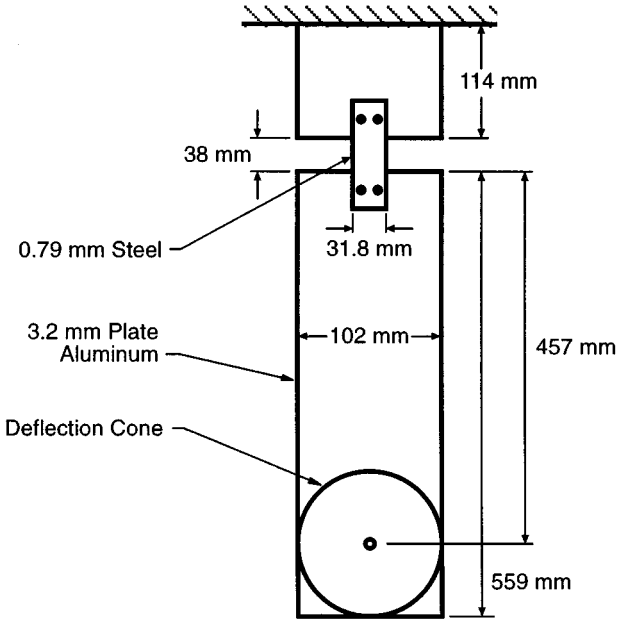

FIG. 3. Dimensions of compound cantilevered beam.

This implies that, for comparable bending moments, the maximum strain in the steel beam is 75 times that experienced in the aluminum beam.

The bending moment in the strain-sensing beam is measured via Entran model ESU-025-500 P-type silicon strain gages. This type of strain gage has a gage factor of 140, which is approximately 70 times greater than that of common foil strain gages. The P-type silicon gages were specified to achieve higher strain resolution than is possible with ordinary gages, a necessity due to the small magnitude of the forces involved (strains of less than 20 μm/m were expected). Four gages were used in a conventional fully active bridge configuration. These gages require special mounting techniques and materials that are specified by the manufacturer. Figure 4 shows the configuration of the strain-sensing beam. Refer to Appendix A for calculation of strains for the compound beam configuration.

D. Signal conditioner

The strain gage leads are connected to the signal conditioning electronics by a 4 twisted-pair shielded cable. To facilitate modular design, the cable terminates in a 9-pin D-subminiature connector that can be plugged into the bridge amplifier unit. An Analog Devices model 1B32AN bridge transducer signal conditioner was used to operate the strain gage bridge. The 1B32AN is capable of providing a 4 to 15 V bridge excitation source. Its amplifier gain is adjustable from 100 to 5000 V/V and is programmed externally on a prototype board. The signal conditioner contains a low pass filter with a 4 Hz cutoff frequency that reduces the effects of both noise and unsteadiness in the force measurement.

The 1B32AN requires external circuitry for gain settings, offset settings, power, etc. A circuit diagram of the entire bridge and signal conditioner assembly is shown in Fig. 5.

The ± 10 V output of the bridge signal conditioner is displayed using a Newport model 2001A-4 voltmeter. This

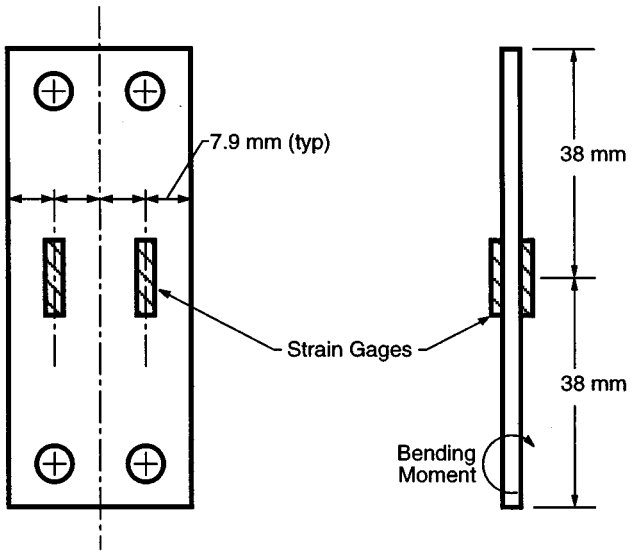

FIG. 4. Schematic of strain sensing beam.

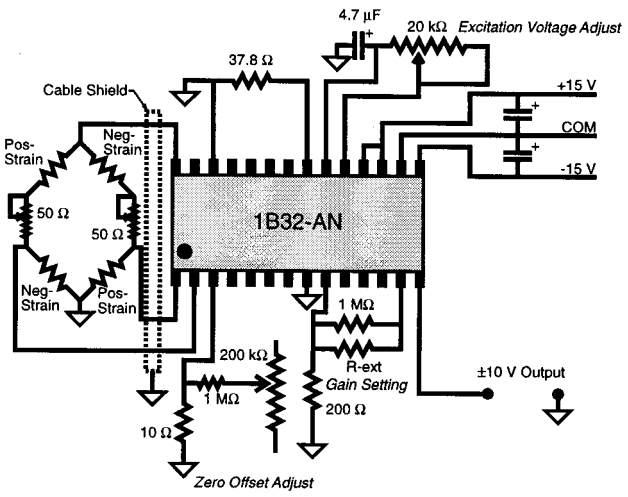

FIG. 5. Circuit diagram of strain gage bridge and signal conditioning electronics.

voltmeter has a range of ±20 V with 0.001 V resolution. The 1B32AN offset was adjusted to approximately −10 V for the undeflected beam. This allows the maximum possible range and resolution.

E. Damping mechanism

Our damping mechanism provides the remaining key advantage of this instrument. Damping is required because, at low momentum rates, even minor oscillations of the mass suspended by the beam can overwhelm the force measurement. Since only steady state sprays will be considered when using this instrument, there is no strict requirement for dynamic response. This allows use of significant damping. In an early version of the instrument, an AirPot model 50047 air dashpot was used. However, it was found that friction between the moving dashpot parts caused significant hysteresis in the cantilevered beam. The dashpot was therefore replaced by a viscous fluid damper.

The viscous fluid damper consists of a paddle attached to the end of the lower rigid beam. Motion of the beam causes the paddle to move within a close-fitting container filled with 0.90 kg/m s glycerine. Glycerine was chosen because of its availability, high viscosity, and low volatility. The fluid shear occurring within the small clearances causes the desired damping effect. Neglecting the very small effects of (1) surface tension, calculated in the worst case to be approximately 0.001 N, or about 1% of full scale for the range setting used here, and (2) fluid yield stress, negligibly small for glycerine, static friction is virtually absent.

F. Effervescent atomizer

The effervescent atomizer used to produce the sprays that were investigated using the momentum rate probe is shown schematically in Fig. 6. Spray liquid and atomizing gas are injected into the nozzle mixing chamber where a two-phase mixture is formed. This mixture flows through the nozzle exit orifice and the expanding atomizing gas causes rapid atomization. The nozzle exit orifice section is

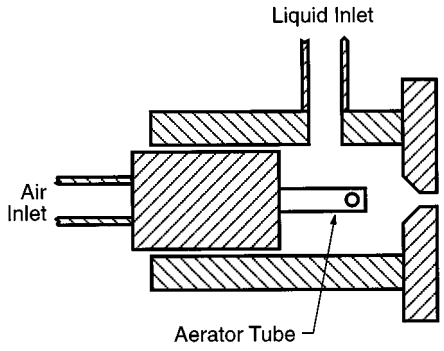

FIG. 6. Schematic of effervescent atomizer.

interchangeable—0.38- and 0.51-mm-diam orifices were used during this study. The atomizer can deliver a liquid flow rate of approximately 0.5 to 1.5 g/s. The atomizing gas flow rate is characterized by the gas-to-liquid mass flow ratio (GLR). GLR's for effervescent sprays typically range from 1% to 10%.

G. Gas/liquid supply system

The liquid and gas supply systems for the effervescent atomizer are shown in Fig. 7. These systems are used in the calibration phase, when only liquid is fed to the nozzle, and in the data acquisition phase, when both liquid and gas are required. Rotameters are used to monitor the liquid and gas mass flow rates. Liquid flow rates were monitored using an Omega FL-114 rotameter with a stainless steel float. This rotameter has a range of 0.4 to 2.0 g/s for the liquids used here and a resolution of approximately 0.04 g/s. A Brooks R-2-15A rotameter was used to monitor gas flow rates. This rotameter is capable of handling air flow rates from 0.008 to 0.08 g/s with a resolution of 0.0008 g/s. A pressurized sphere was used as a liquid reservoir for the system. Dried, high pressure air was used as the atomizing gas and to pressurize the liquid reservoir.

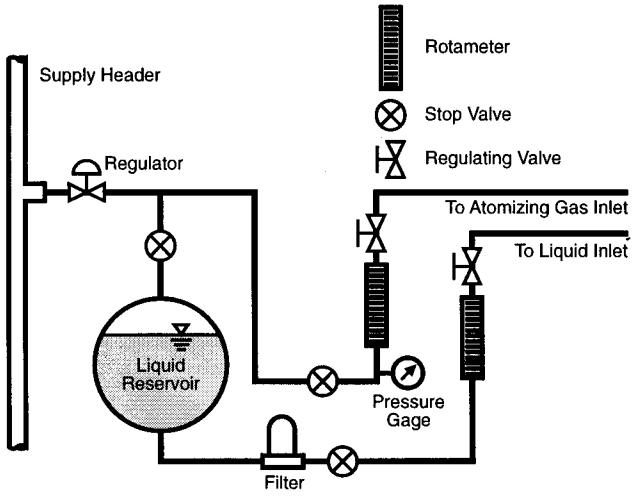

FIG. 7. Schematic of effervescent atomizer supply system.

H. Nozzle traverse

The effervescent atomizer was mounted horizontally on a two-dimensional traverse capable of motion in the plane normal to the spray axis. The traverse made it possible to align the spray axis with the tip of the deflection cone. This alignment was performed visually, since slight misalignment has little effect on the moment applied to the end of the strain-sensing beam (<0.4% for 1 mm of misalignment). Since the tip of the deflection cone has a finite width, the spray must be located a sufficient distance (8 to 12 mm) away from the tip to prevent the dense, developing region of the spray from impinging on it. Otherwise, much of the spray will be partially deflected by the probe tip, adversely affecting data quality. The nozzle to probe tip separation must be determined by trial and error, since it varies with spray configuration and probe tip width.

I. Exhaust system

The momentum rate probe was suspended from a frame that was located above an exhaust system. Most of the spray liquid impinged upon the deflection cone and drained vertically downward off the cone into the exhaust sump. However, since some of the spray remained airborne after being deflected radially outward or vertically upward, some shielding was necessary to contain the overspray in the work area. An exhaust blower was therefore employed to remove airborne spray particles, since many were respirable. The blower damper was closed as far as possible to minimize any extraneous motion of the cantilevered beam caused by drafts. The exhaust draft caused a slight (1%) change in the zero of the instrument, but since the momentum rate versus voltage curve is linear (as will be shown below), this effect is easily eliminated by taking a new zero reading when the blower is operating.

III. EXPERIMENTAL PROCEDURE

A. Calibration

The forces measured by the momentum rate probe are equivalent to the weight of approximately 4 g. Since the cantilevered beam is vertical, a calibration weight would require some turning mechanism for producing a horizontal force. Such a mechanism would inevitably introduce frictional forces. A system reliant on calibration weights, therefore, would be impractical and inaccurate. Instead, a liquid jet with a known velocity profile was used as a calibration standard. Since the momentum rate of a liquid jet is easily calculated, this method is an accurate means of calibrating the momentum rate probe for low mass flow rate sprays.

Before the calibration procedure is performed, it is necessary to determine the range of forces that must be measured by the probe. Prior to this investigation, little data existed on the velocities in the near nozzle region of the two-phase flow, so the proper gain setting for the bridge signal conditioner was determined by trial and error. The spray nozzle was operated at the highest flow rate and GLR in the test matrix, and the gain was adjusted to obtain the full scale +10 V output. The sprays examined here required the use of an amplifier gain of 300, which resulted in a range of approximately 0.01 to 0.08 N.

The calibration curve was generated by spraying only liquid from the nozzle at various mass flow rates. The velocity profile at the nozzle exit was classified as either fully developed or slug flow based on developing flow calculations.[10,11] This classification is necessary to accurately calculate the momentum rate of the liquid stream. Using this classification scheme, the maximum error in the calculated momentum rate (for the case where the liquid viscosity and flow rate are such that the velocity profile is partially developed) is approximately 15%, as shown in the following section.

Calibration curves were generated before and after the spray data were collected to ensure that no significant change in instrument sensitivity had occurred. Figure 8 shows a sample calibration curve. The fluid was SNO-320, a hydrocarbon oil, and both the 0.38- and 0.51-mm-diam nozzle orifices were used. A least-squares line has been fitted to the calibration points. Note that the scatter is quite small, with a coefficient of determination (r^2) of 0.997.

B. Data collection

After a calibration curve had been generated for the momentum rate probe, spray data were collected. This required simply setting the appropriate atomizer gas and liquid mass flow rates and recording the bridge signal conditioner voltage output when the instrument reached steady state. The settling time for the momentum rate probe depends strongly on mechanical damping of the beam and the response time of the electronics. The configuration described here has a settling time of approximately 5 s, due almost entirely to the mechanical characteristics of the system. The spray was turned off at approximately 10 min intervals to record a new tare voltage, since the zero of the instrument may drift

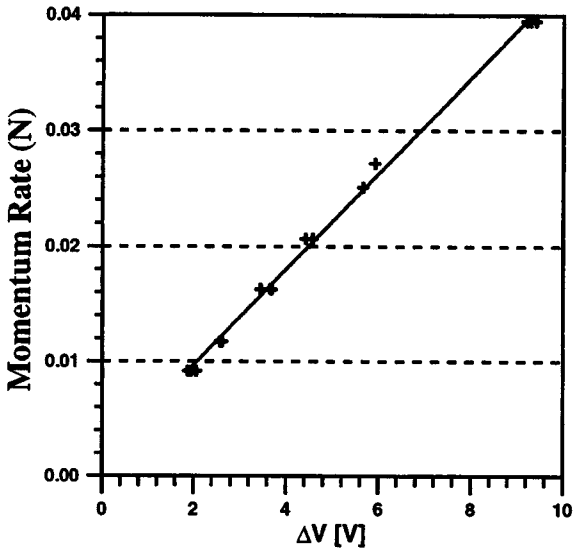

FIG. 8. Sample calibration curve for momentum rate probe.

slightly (approximately 2%) over this interval. This is probably due to temperature variations in the bridge and amplifier.

Figure 9 presents spray momentum rate data for SNO-320 sprays using both nozzle orifices. This plot shows that momentum rate is nearly linear with GLR for each liquid mass flow rate and nozzle diameter. Again, the data points have been fitted with straight lines. The coefficients of determination for these fits range from 0.991 to 0.998.

C. Experimental uncertainty

Uncertainty in the momentum rate measurement results from three sources. The first is error in the calibration liquid flow rate. The momentum rate is proportional to the square of the liquid mass flow rate, so the momentum rate uncertainty is approximately twice that of the liquid flow rate. For the rotameter used here, the contribution to the momentum rate uncertainty is approximately 4% of the rotameter's full scale value.

The second source of uncertainty results from the method used to calculate liquid jet momentum rate. For some liquid jet Reynolds numbers, the jet velocity profile is partially developed and thus lies between the fully developed and plug flow limiting cases. Since the degree of flow development could not be accurately determined in some cases, partially developed jets were classified as either fully developed or slug flows. This classification introduces no more than 15% error for individual data points because (1) the momentum rate difference between fully developed and slug flows is 30% and (2) a partially developed flow can at worst lay halfway between these limiting values. Thus, the fully developed or plug flow assumption contributes less than 15% uncertainty (approximately 5% of the rotameter's full scale value) to the overall calibration.

The final source of uncertainty in the momentum rate measurement results from fluctuations in the strain gage bridge readout. These fluctuations occur despite the inclusion of the viscous fluid damper. The 95% confidence interval associated with the strain gage readout is approximately ± 0.4 V, or 2% of readout's full scale value.

Assuming that the three errors listed above are normally distributed and act independently, the overall uncertainty (rms of individual uncertainties) in the momentum rate measurements is approximately 7% of the instrument's full scale value (about 5×10^{-3} N).

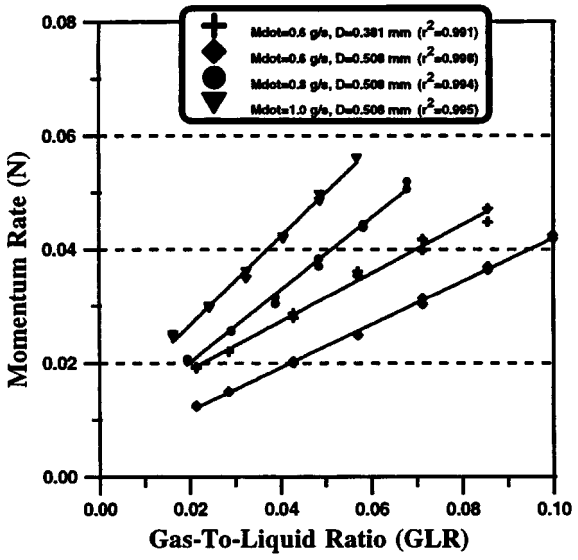

FIG. 9. Plot of momentum rate vs gas-to-liquid ratio by mass (GLR).

NOMENCLATURE

	Description and units
a	distance along deflection cone axis of symmetry, m
b	strain-sensing beam width, m
B	constant, l/s
E	modulus of elasticity, N/m^2
EI	beam stiffness, N m^2
F	similarity function, dimensionless
g	gravitational acceleration, m/s^2
GLR	gas-to-liquid ratio, dimensionless
h	strain-sensing beam thickness, m
I	section moment of inertia, m^4
l	distance along rigid beam, m
L	length of rigid beam, m
m	mass, kg
M_R	moment, N m
p	pressure, Pa
r	radial distance from deflection cone axis of symmetry, m
u,v	axial and radial velocities, m/s
x	flow streamwise coordinate, m
y	distance along deflection cone axis of symmetry, m
z	flow transverse coordinate, m
ϵ	strain, dimensionless
η	axial coordinate, dimensionless
μ	fluid viscosity, kg/m s
ν	kinematic viscosity, m^2/s
θ	angle of deflection, rad
ρ	fluid density, kg/m^3
σ	stress, N/m^2
ψ	stream function, m^3/s
ψ^*	dimensionless stream function
Subscripts	
A	probe tip
R	rigid beam bending axis
1	rigid beam center of mass
2	to deflection cone axis of symmetry

APPENDIX A: BEAM DEFLECTION CALCULATION

The purpose of this calculation is to determine the required sensitivity of the strain gages and signal conditioning electronics. The strain in the strain-sensing beam is calculated using a static moment balance. The free body diagram used for this analysis is shown in Fig. 10. The principle equation is

$$\sum \mathbf{M}=\mathbf{0} \quad \text{(about origin)} \tag{A1}$$

which, expressed as a scalar equation is

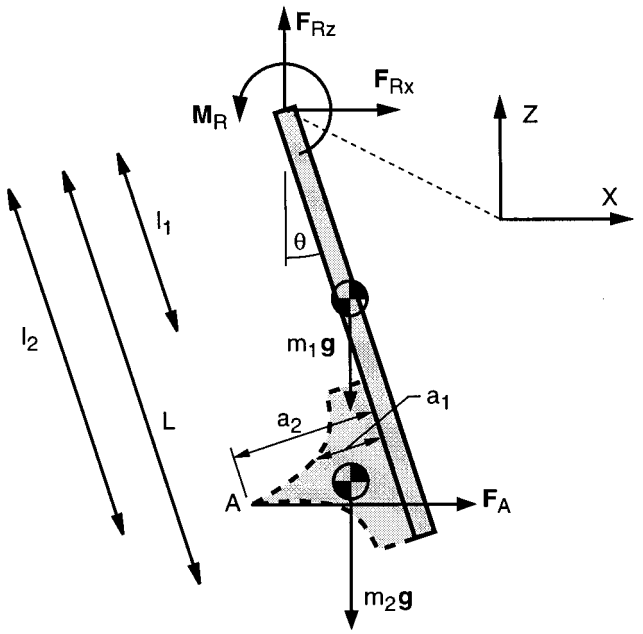

FIG. 10. Free body diagram of rigid beam and deflection cone. Note that the strain-sensing beam supplies the reaction force and moment at the top of the rigid beam.

$$M_R - m_1 g l_1 \sin(\theta) - m_2 g[l_2 \sin(\theta) - a_1 \cos(\theta)] + F_A[l_2 \cos(\theta) + a_2 \sin(\theta)] = 0, \tag{A2}$$

where M_R is the reaction moment at the top of the rigid beam where the strain-sensing beam is attached. F_A is the force imparted to the probe by the spray at point A. Also in Eq. (A2), m represents the mass of the members, a and l are lengths, θ is the angle of deflection, and g is the acceleration of gravity, all as defined in Fig. 10. The slope at the end of the strain-sensing beam can be expressed as

$$\tan(\theta) = -\frac{M_R L}{EI}, \tag{A3}$$

where E is the modulus of elasticity and I is the section moment of inertia. This results in an implicit equation for θ:

$$\frac{Ebh^3}{12L}\tan(\theta) = [m_1 g l_1 + m_2 g l_2 - F_A a_2]\sin(\theta) - [m_2 g a_1 + F_A l_2]\cos(\theta), \tag{A4}$$

where b and h are, respectively, the width and thickness of the strain sensing beam. The maximum stress in the beam is

$$\sigma_{\max} = \frac{M_R(h/2)}{I} = -\frac{EI \tan(\theta)(h/2)}{LI} \tag{A5}$$

and the maximum strain is

$$\epsilon_{\max} = \frac{\sigma_{\max}}{E}. \tag{A6}$$

This strain can be used to specify the sensitivity of the strain gage bridge and signal conditioning electronics.

APPENDIX B: DEFLECTION CONE CONTOUR

This is a brief discussion of the calculations made to obtain the contour of the deflection cone. An analysis of an axisymmetric stagnation flow begins with the Navier–Stokes equations in cylindrical coordinates:

$$u\frac{\partial u}{\partial r} + v\frac{\partial u}{\partial y} = -\frac{1}{\rho}\frac{\partial p}{\partial r} + v\left\{\frac{1}{r}\frac{\partial}{\partial r}\left(r\frac{\partial u}{\partial r}\right) - \frac{u}{r^2} + \frac{\partial^2 u}{\partial y^2}\right\}, v; 4q \tag{B1}$$

$$u\frac{\partial v}{\partial r} + v\frac{\partial v}{\partial y} = -\frac{1}{\rho}\frac{\partial p}{\partial y} + v\left\{\frac{\partial^2 v}{\partial r^2} + \frac{1}{r}\frac{\partial v}{\partial r} + \frac{\partial^2 v}{\partial y^2}\right\}. \tag{B2}$$

The stream function is utilized, with the appropriate definitions for cylindrical coordinates:

$$u = -\frac{1}{r}\frac{\partial \psi}{\partial y}, \quad v = \frac{1}{r}\frac{\partial \psi}{\partial r}. \tag{B3}$$

The stream function for inviscid stagnation point flow is given by

$$\psi = -Br^2 y. \tag{B4}$$

This stream function is modified to satisfy the no-slip boundary condition at the wall by defining the following similarity variable and stream function, which have been nondimensionalized:

$$\eta = y\sqrt{\frac{B}{\nu}}, \quad \psi^* = -r^2 F(\eta)\sqrt{B\nu}. \tag{B5}$$

Substitution of these expressions into the momentum relations reveals that the r coordinate dependence vanishes and that the profile can be expressed as the dimensionless ordinary differential equation

$$\frac{d^3 F}{d\eta^3} + 2F\frac{d^2 F}{d\eta^2} - \left(\frac{dF}{d\eta}\right)^2 + 1 = 0. \tag{B6}$$

This equation is solved for η numerically using the appropriate boundary conditions as discussed in detail by White.[6]

After the solution for η is obtained, the dimensional value y is calculated. This requires knowledge of values for the mixture kinematic viscosity and the scaling parameter B.

The kinematic viscosity ν is estimated assuming homogeneous two-phase flow. Considering air–liquid ratios between 0.02 and 0.06 for atmospheric pressure air and water gives a mixture density between 20 and 60 kg/m^3. The mixture dynamic viscosity can be modeled as that of parallel liquid and air sheets aligned with the flow (in the case of an annular two-phase flow at the nozzle exit) or parallel liquid and air sheets aligned perpendicular to the flow (in the case of bubbly or slug flow at the nozzle exit).[12] No slip between the air and liquid flows is assumed, since the slip ratio is not known *a priori*. The choice of two-phase flow regime has some effect on the calculated value of μ—it ranges from 1.8×10^{-5} to 1.9×10^{-5} kg/m s for the parallel liquid and air sheets aligned with the flow and from 3.8×10^{-5} to 7.6×10^{-5} kg/m s for the parallel liquid and air sheets aligned perpendicular to the flow. Both situations are likely to be of

interest, so a compromise value of $\mu=3.8\times10^{-5}$ kg/ms was chosen. Combining μ and ρ gives ν values ranging from 3×10^{-7} to 3×10^{-6} m^2/s. Again, a compromise value was determined: $\nu=1.2\times10^{-6}$ m^2/s.

The stream function scaling parameter B was estimated from a continuity analysis, where the flow at the nozzle exit plane was assumed to be inviscid. There are two reasons for making this assumption. First, as shown in the previous paragraph, the mixture viscosity is low. Second, the nozzle exit plane is located sufficiently far upstream of the deflection cone so that viscous effects due to the stagnation flow boundary layer are absent. Subsequent calculations using the viscous flow equations (B5) and (B6) support this conclusion.

Application of continuity requires knowledge of the mixture density and mixture velocity at the atomizer exit orifice. The former is known, while the latter is estimated by using the diameter of the atomizer exit orifice (0.38 or 0.51 mm) and the range of mass flow rates of interest (0.3 to 1.5 g/s). This yields mixture velocities ranging from 40 to 660 m/s and B values from 400 to 3300 s^{-1}. A compromise value of 2000 s^{-1} was chosen for B, based on the prevalence of cases run near this condition.

The last step required when transforming the similarity solution to physical dimensions is to identify the streamline that is tangent to the cone surface. In our case, machining tolerances limited the diameter of our probe tip to 1.52 mm (0.060 in.). We therefore assumed that the incoming streamline was nearly vertical (deviation from vertical of less than 0.5°) when it reached the probe tip ($r=1.52$ mm). This requires a probe tip altitude of slightly more than 4.3 cm.

Finally, the diameter of the deflection cone base is chosen. In our work, it was sized such that the streamlines are turned through nearly 90° (89.5° to be consistent with the inflow constraint) within this diameter. Based on arguments from the previous paragraph, this results in a diameter of slightly more than 8.7 cm.

[1] M. T. Lund, P. E. Sojka, A. H. Lefebvre, and P. G Gosselin, Atom. Sprays **3**, 77 (1993).
[2] S. G. Bush and P. E. Sojka, ASME FED **178** HTD **270**, 117 (1993).
[3] E. Giffen and T. F. Crang, Proc. Inst. Mech. Eng. **215**, 83 (1946).
[4] W. J. Klingebeil and R. W. Moulton, AIChE J. **17**, 383 (1971).
[5] M. Deichsel and E. R. F. Winter, Int. J. Mult. Flow **16**, 391 (1990).
[6] F. M. White, *Viscous Fluid Flow*, 2nd ed. (McGraw–Hill, New York, 1991).
[7] K. Hiemenz, Dingler's Polytech. J. **326**, 321 (1911).
[8] F. Homann, Z. Agnew. Math. Mech. **16**, 153 (1936).
[9] F. P. Beer, and E. R. Johnston, *Mechanics of Materials* (McGraw–Hill, New York, 1981).
[10] W. M. Roshenow and H. Y. Choi, *Heat, Mass, and Momentum Transfer* (Prentice–Hall, Englewood Cliffs, 1961).
[11] H. L. Langhaar, J. Appl. Mech. **June** A55 (1942).
[12] G. B. Wallis, *One-Dimensional Two-Phase Flow* (McGraw–Hill, New York, 1969).